A&A 635, A44 (2020)
https://doi.org/10.1051/0004-6361/201937307

Astronomy & Astrophysics

Bimodal distribution of the solar wind at 1 AU

C. Larrodera and C. Cid

Space Weather Research Group, Departamento de Física y Matemáticas, Universidad de Alcalá, A-2, km 33,600, Alcalá de Henares, Spain
e-mail: carlos.larrodera@edu.uah.es, consuelo.cid@uah.es

Received 13 December 2019 / Accepted 29 January 2020

ABSTRACT

Aims. Here we aim to separate the two main contributions of slow and fast solar wind that appear at 1 AU.
Methods. The bi-Gaussian function is proposed as the probability distribution function of the two main components of the solar wind. The positions of the peaks of every simple Gaussian curve are associated with the typical values of every contribution to solar wind. We used the entire data set from the Advanced Composition Explorer (ACE) mission in an analysis of the data set as a whole and as yearly series. Solar cycle dependence is considered to provide more accurate results for the typical values of the different parameters.
Results. The distribution of the solar wind at 1 AU is clearly bimodal, not only for velocity, but also for proton density, temperature and magnetic field. New typical values for the main parameters of the slow and fast components of the solar wind at 1 AU are proposed.

Key words. Sun: heliosphere – solar wind

1. Introduction

The observations of the solar wind made during the Mariner 2 flight to Venus in 1962 discovered streams of hot, high-velocity plasma recurring at intervals of 27 days (Neugebauer & Snyder 1966). Between streams the proton velocity dropped as low as 307 km s^{-1} from an average value of approximately 500 km s^{-1}. These were just the first observations of the two main contributions to solar wind: the fast flow, from coronal holes, and the slow wind, with a less certain origin (Abbo et al. 2016). Transient ejections with a wide range of velocities are also contributing to the solar wind observed at 1 AU.

Typical features of slow and fast components of the solar wind at 1 AU have been summarised by several authors (see reviews by Bothmer & Zhukov 2007; Hansteen 2010 and references therein). Based on the statistical analysis of samples from different missions, all authors agree that fast wind is hotter and less dense than slow solar wind, but some discrepancies appear when comparing the values of the basic parameters of both types of solar wind (see Table 1). One of the differences is that magnetic field strength is the same for both contributions according to Hansteen (2010) while some differences appear for Bothmer & Zhukov (2007). Although these differences are included in the uncertainty on the value provided by Hansteen (2010), it would be useful to know whether the magnetic field strength presents some differences between both components of solar wind.

Comparing the interplanetary magnetic field along the solar cycle, Hirshberg (1969) reported high tails in the distribution function of the magnitude of the interplanetary magnetic field (B) during a period of rising solar activity (1966–1967). However, no tail was seen during solar minimum (1963–1964). The tails in the distribution functions of solar wind plasma and magnetic field were attributed to solar mass ejections and the compression of solar wind regions of different speeds (Neugebauer & Snyder 1966; Hirshberg 1969).

Burlaga & King (1979) were the first to suggest that the distribution of the logarithm of B data could be well represented as normally distributed. The analysis of skewness and kurtosis of the log B for years 1973–1990 allowed Feynman & Ruzmaikin (1994) to demonstrate that the distribution of logarithms of one-hour averaged B is non-Gaussian. Nevertheless, the lognormal distribution has been used extensively to describe not only B, but also solar wind speed, density and temperature (e.g. Burlaga & Szabo 1999; Burlaga 2001; Veselovsky et al. 2010; Venzmer & Bothmer 2018).

The lognormal distribution was considered as proof of a lack of separation between fast and slow flows at 1 AU, describing the solar wind as a simple statistical structure resulting from the dynamical evolution and interaction of the flows at 1 AU (Burlaga & Szabo 1999; Burlaga 2001). Moreover, Venzmer & Bothmer (2018) noted that the lognormal distribution appears to be better at describing the shape of the IMF, the density and the temperature distributions than at describing the solar wind speed. Therefore these latter authors considered a bi-component lognormal for the velocity distribution with a better result.

Other approaches to the distribution function of magnetic field strength, or other solar wind plasma parameters, consist in using the kappa-like distributions, adding in some cases artificial terms to make the symmetric distribution more skewed (Burlaga & Viñas 2004). Kappa-like distributions with fat tails can be obtained as a superposition of random uncorrelated, normally or lognormally distributed processes (Vörös et al. 2015) in the context of non- extensive (non-additive) statistical mechanics. Also a randomised Weibull probability distribution function (PDF) was proposed for the magnetic field intensity (Consolini et al. 2009).

The historical evolution described above regarding the analysis of the distribution function of the solar wind parameters shows that more complex mathematical functions are being implemented as time passes assuming that the mixing and dynamical interaction makes separating the different components of the solar wind at 1 AU impossible. Nevertheless, slow and fast solar wind intervals are clearly identified at 1 AU.

Table 1. Typical values for the parameters of the slow and fast components of the solar wind.

	V_p (km s^{-1})	B (nT)	n_p (cm^{-3})	T_p ($\times 10^5$ K)	
Slow wind	$\lesssim$450	4	7–10	0.4	Bothmer & Zhukov (2007)
	430 ± 100	6 ± 3	$\simeq$10	0.4 ± 0.2	Hansteen (2010)
Fast wind	450 – 800	5	3	2	Bothmer & Zhukov (2007)
	700 – 900	6 ± 3	$\simeq$3	2.4 ± 0.6	Hansteen (2010)

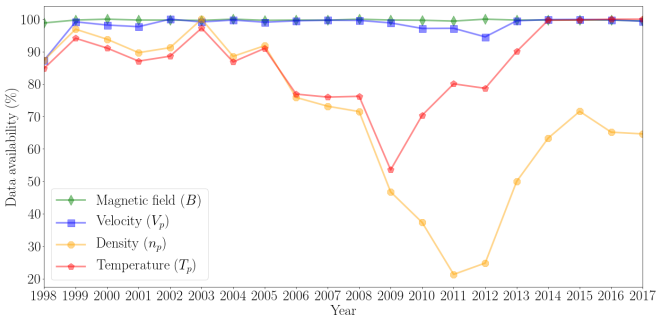

Fig. 1. Data coverage of the main solar wind parameters measured by the ACE spacecraft from the time it is operational until the end of the year 2017.

In order to identify the solar sources of individual packets of solar wind, Stansby et al. (2018) used solar wind measurements closer to the Sun than 1 AU, where the mixing and dynamical interaction of different solar wind streams is reduced. After removing all the intervals identified as coronal mass ejections from the data, these latter authors found three different populations at 0.3 AU, corresponding to wind that originated: (1) in the core of coronal holes, (2) in or near active regions or edges of coronal holes, and (3) in small transients. On the other hand, the first observations from the Parker Solar Probe at 36 to 54 solar radii show evidence of slow Alfvénic solar wind emerging from a small equatorial coronal hole (Bale et al. 2019).

In this paper we separate the two main components of solar wind at 1 AU, fast and slow flows, from other contributions to the distribution function of the observed values of the main parameters of the solar wind measured by the Advanced Composition Explorer (ACE) spacecraft. The ACE data are described in Sect. 2, and the bi-Gaussian approach with the statistical results and the solar cycle dependence are presented in Sect. 3. Finally, Sect. 4 discusses the results and Sect. 5 summarises our conclusions.

2. Data

This study uses data from the ACE spacecraft. The ACE mission orbits the L1 point, and has a prime view of the solar wind accelerated by the Sun. Data used here were measured by the Solar Wind Electron, Proton, and Alpha Monitor (SWEPAM; McComas et al. 1998) and the Magnetic Field Experiment (MAG; Smith et al. 1998) on board the ACE spacecraft. The level 2 data from SWEPAM and MAG were obtained from the ACE Science Center[1].

The ACE spacecraft provides continuous coverage of solar wind parameters since early 1998, although with some data gaps in SWEPAM data during periods of high solar activity. In this study we use the entire hourly data set from 23 January 1998 to December 2017 (about two solar cycles, namely 23 and 24). The data set includes the proton density, n_p, the radial component of the proton temperature, T_p and the proton speed, V_p, from SWEPAM, and the magnetic field magnitude, B from MAG.

The data coverage of different solar wind parameters is shown in Fig. 1. We highlight the good coverage of the magnetic field magnitude and the proton speed many years past the original planned mission lifetime. Figure 1 also shows that, as informed by the SWEPAM instrument team, the proton density, and to a lesser extent the temperature, became increasingly sparse starting in 2010 as the detectors aged. Since 23 October 2012, an operational improvement has significantly increased the frequency of good-quality SWEPAM observations.

3. A bi-Gaussian approach

Considering the recent results from Parker Solar Probe (Bale et al. 2019), both slow and fast contributions to solar wind emerge from coronal holes, small or large, respectively. Therefore, the simplest model for the solar wind consists in two flows from two coronal holes (one large and one small) with different speeds (one fast and one slow) emerging from the Sun. Nevertheless we should be aware that not all large (or small) coronal holes present the same size. Small changes in this size are expected to result in small changes in the speed of the emerging flow. Indeed, Garton et al. (2018) show that the longitudinal width of coronal holes presents a strong correlation with the peak of the solar wind speed measured by ACE. Also the speed of a flow can be modified during the propagation until reaching 1 AU.

Here we use a bi-Gaussian approach as the probability distribution function of the two main components of solar wind at 1AU (slow and fast flows). This function provides the mathematical framework for the physical model described above.

The bi-Gaussian is defined as the addition of two Gaussian (or normal) distribution functions, one for the fast wind and another for the slow wind, as is given by

$$bG(x) = h_1 \cdot \exp\left(\frac{-(x-p_1)^2}{2w_1^2}\right) + h_2 \cdot \exp\left(\frac{-(x-p_2)^2}{2w_2^2}\right) \quad (1)$$

where x is V_p, n_p, T_p or B depending on the selected data set. Here, h_1, p_1, w_1, h_2, p_2 and w_2 are the six parameters obtained when fitting the bi-Gaussian distribution function to a data set. The subscripts 1 and 2 correspond to the normal distribution of each component of the solar wind. Be aware that 1 and 2 do not always correspond to slow and fast wind, respectively. Here h is the height of the peak of each single Gaussian curve, p is the position of the centre of the peak and w is the Gaussian rms width of each single curve.

3.1. Statistics with the whole data set

Figure 2 shows the empirical distribution functions of the selected solar wind parameters, V_p, n_p, T_p or B, for the whole data set available from ACE and the fitting to a bi-Gaussian. The

[1] www.srl.caltech.edu/ACE/

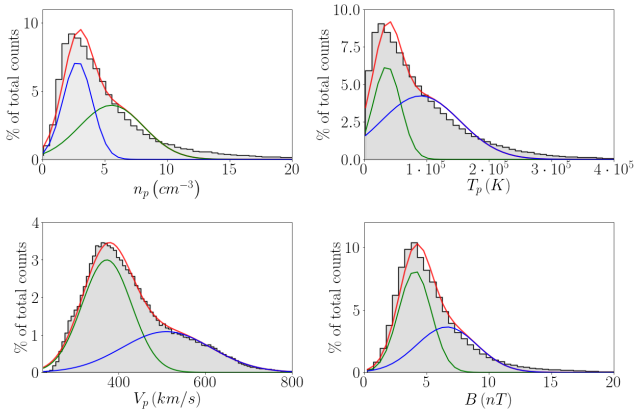

Fig. 2. Empirical distribution functions of the main solar wind parameters, n_p, T_p, V_p, and B, for the whole data available from ACE and the fitting to a bi-Gaussian (red). Green and blue lines correspond to the single Gaussian curves.

two single Gaussian curves also appear as the blue and green lines.

The Pearson chi-square (hereafter χ^2) has been used to quantify the goodness of fit, as the size of the sample is large enough to accurately use this goodness of fit test. The χ^2 is calculated using $\chi^2 = \sum_{i=1}^{k} (O_i - E_i)^2 / E_i$, where O_i is the number of values of a PDF falling into the ith interval and E_i is the expected number of values considering the theoretical function (Eq. (1)) for the same interval (Suhov & Kelbert 2014). The χ^2 values obtained appear in the last column of Table 2, ranging from 0.02 for V_p to 21.77 for n_p, indicating that the best (worse) fitting corresponds to the proton speed (density). In any case, the values obtained allow us to claim that the fitting of a bi-Gaussian is appropriate for the PDFs of all the solar wind parameters analysed. This fact suggests that two solar wind populations can be distinguished, not only in the proton speed, but also in n_p, T_p and B.

Most of the proton speed is spread around 370 km s^{-1}, but there is also a significant fraction of data spread around 510 km s^{-1}, corresponding to slow and fast contributions to the solar wind, as expected. Other values corresponding to the different solar wind parameters are in Table 2.

The tails, which are not completely reproduced by the bi-Gaussian, are expected to be related to solar transients and the compression of solar wind regions of different speeds (Wimmer-Schweingruber et al. 2006). However, data collected during these time intervals are not statistically significant. Indeed, when computing how much the real distribution function departs from the bi-Gaussian on the right side of the graphs (i.e. computing the amount of data which are left above the bi-Gaussian on that side), we obtain values which range from 0.4% for the solar wind velocity up to 9% for the proton density.

To identify which one of the two Gaussian curves (1 or 2) corresponds to each component of the solar wind (slow or fast), we compare the position of the centre of the peak of every single Gaussian curve, p, with the values in Table 1. The peak of the first (second) Gaussian curves of V_p, B and T_p fits well with the values for the slow (fast) contribution in Table 1. On the contrary, the peak of the second (first) Gaussian curve of n_p is the one which agrees with the slow (fast) contribution.

Thus, considering the position of the peak of every Gaussian as the value for a magnitude of a type of solar wind, with an uncertainty equal to the spread of the data around the peak, that is, equal to the rms of the curve, we obtain the main parameters of each contribution to the solar wind at 1 AU (see Table 3).

3.2. Yearly data sets and solar cycle dependence

Here we decipher whether or not the values obtained for the two contributions of the main solar wind parameters (Table 3) change over time. Specifically we are interested in the dependence of the centre of the peak of the first and the second Gaussian curves (p_1 and p_2) on the solar cycle. For this purpose, we fitted the empirical yearly PDFs of V_p, n_p, T_p and B to a bi-Gaussian function.

Figure 3 compares the evolution of p_1 and p_2 for the main solar wind parameters to the yearly sunspot number (SSN) from WDC-SILSO as a proxy of the solar cycle. Shadowed areas in the different panels are centred at the weighted average of the peak of corresponding Gaussian curve and extend to $\pm\sigma$ (see Table 4). Grey (red) colour corresponds to the slow (fast) contribution to solar wind.

The Pearson's correlation coefficient, r, between p_B^1 or p_B^2 and the SSN are above 0.7, and between p_N^1 or p_N^2 and the SSN are above 0.65. Therefore, the magnetic field strength and the proton density of both slow and fast solar wind contributions are strongly related to the solar cycle. Figure 4 shows the scatter plots of the yearly position of the peak for B and n_p versus the sunspot number along with the linear fit. For p_V^1, the correlation coefficient is 0.5, indicating a weak correlation. No correlation appears in other cases, as the correlation coefficients are below 0.1.

4. Discussion

In the previous section the bi-Gaussian function was applied to reproduce the bulk solar wind at 1 AU (see Fig. 2). The main solar wind parameters measured by ACE are properly reproduced by the bi-Gaussian function, showing that the bulk solar wind can be described using a bi-modal approach. This result disagrees with the description of the solar wind as a simple statistical structure originating from the dynamical evolution and interaction of the flows at 1 AU (Burlaga & Szabo 1999; Burlaga 2001).

The values for the parameters of the slow and fast components of the solar wind from the bi-Gaussian fit (Table 3) agree with previous values for the slow and fast contributions to solar wind (see Table 1) provided by Bothmer & Zhukov (2007). Nevertheless, in our results, the fast contribution to solar wind is slightly colder. When comparing with the values from Hansteen (2010), we obtain a slower and colder fast wind. Regarding magnetic field strength, our results in Table 4 show two different values for the slow and fast contributions to solar wind, as in Bothmer & Zhukov (2007), while there is no difference in this parameter for the two contributions in the results by Hansteen (2010).

We checked the bi-modal distribution of the solar wind at 1 AU, not only by using the ACE data set from its entire mission as a whole, but also the yearly data sets. The weighted average of the position of the peaks of the first and the second yearly Gaussian curves (p_1, p_2) of the different solar wind parameters (Table 4) agree with the results from the whole mission.

Considering that the average values have an uncertainty of $\pm\sigma$ (shadowed areas in Fig. 3), we notice that several data points appear out of the shadowed areas. These outliers need to be carefully analysed. Nevertheless, no relationship is perceived between these outliers and the availability of data from ACE during the corresponding year.

In the case of magnetic field strength and proton density, p_1 and p_2 show strong dependence on the SSN. Also, the departure from the shadowed areas for B and n_p can be explained

Table 2. Parameters obtained from the fitting of a bi-Gaussian function to the proton density, the radial component of the proton temperature, the proton speed and the magnetic field strength from the ACE spacecraft since operations began up to 31 December 2017.

	h_1	p_1	w_1	h_2	p_2	w_2	χ^2	Data points
V_p	3.00	373 km s^{-1}	57 km s^{-1}	1.09	510 km s^{-1}	103 km s^{-1}	0.02	172 156
T_p	6.22	3.65×10^4 K	2.20×10^4 K	4.23	9.06×10^4 K	6.31×10^4 K	3.59	148 379
n_p	7.18	2.80 cm^{-3}	1.18 cm^{-3}	3.40	5.53 cm^{-3}	2.58 cm^{-3}	21.77	117 548
B	8.12	4.06 nT	1.31 nT	3.63	6.63 nT	2.42 nT	4.78	175 137

Notes. The χ^2 of the fitting and the number of data points in every sample appear in the two last columns.

Table 3. Values for the main parameters of the slow and fast components of the solar wind at 1 AU from the bi-Gaussian fitting to the whole data set.

	V_p (km s^{-1})	B (nT)	n_p (cm^{-3})	T_p ($\times 10^5$ K)
Slow wind	370 ± 60	4 ± 1	5 ± 3	0.4 ± 0.2
Fast wind	500 ± 100	6 ± 2	3 ± 2	0.9 ± 0.6

Table 4. Same as Table 3 but in this case the values are obtained from the weighted average of the yearly peaks of the first and second Gaussian. Uncertainty corresponds to the weighted standard deviation.

	V_p (km s^{-1})	B (nT)	n_p (cm^{-3})	T_p ($\times 10^5$ K)
Slow wind	376 ± 22	4 ± 1	6 ± 1	0.5 ± 0.3
Fast wind	496 ± 56	7 ± 1	3 ± 1	1.0 ± 0.4

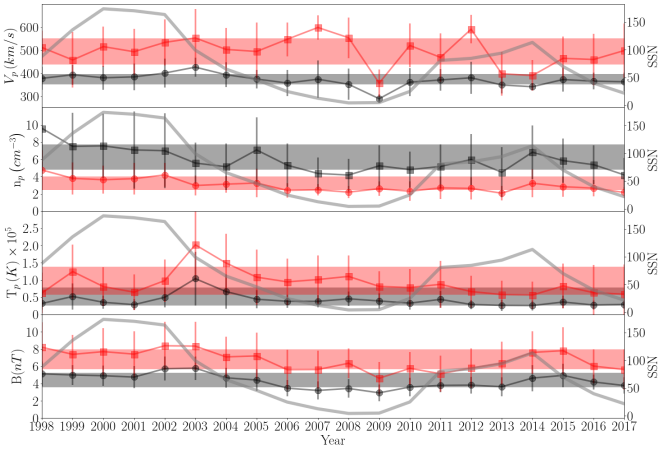

Fig. 3. *From top to bottom*: yearly position of the centre of the peak of every single Gaussian curve, p, for V_p, n_p, T_p and B PDFs. Black (red) points correspond to slow (fast) wind. Uncertainty has been estimated using the Gaussian rms width of the corresponding single curve, w. The grey line in the four plots represents the sunspot number, with the corresponding y-axis on the right of every plot.

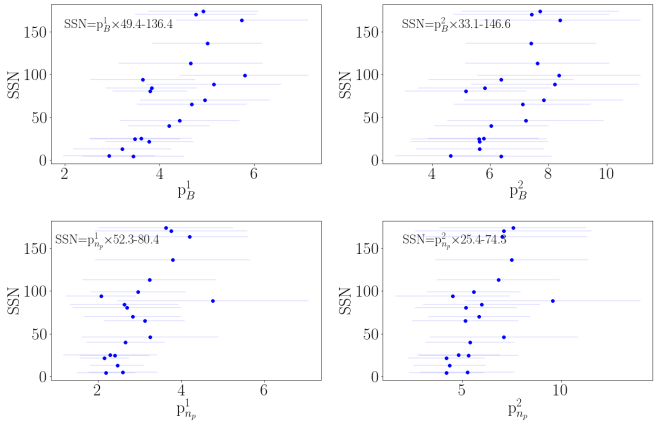

Fig. 4. Scatter plots of the yearly positions of the peak of magnetic field B (*first row*) and proton n_p (*second row*) versus sunspot numbers (SSN). The first (second) column represents the results for the first (second) Gaussian curve. The linear fit equations are shown in the upper-left corner of each plot.

considering their relationship with solar cycle. Therefore, instead of considering a value for the magnetic field and the proton density with a larger uncertainty (e.g. $\pm 2\sigma$), would be useful to obtain a value for slow and fast contributions, not for any time, but for different stages of the solar cycle.

By recalculating for B and n_p, the weighted averages for the two types of wind and different phases of solar cycle (maximum and minimum), we obtain the results that appear in Table 5 (Cols. 3 and 4). The years included in the average for the solar maximum comprise 1998–2003 and 2011–2016. Years from 2006 to 2010 are included in the period to compute the value during the solar minimum. The clear difference obtained in the typical value for B in the different phases of the solar cycle reinforces the results obtained for the whole data sample showing a different typical value for B for slow and fast contributions of solar wind, in agreement with Bothmer & Zhukov (2007)

In the case of those solar wind parameters where no relationship with the solar appears, that is V_p and T_p, even if we extend the shadowed areas to $\pm 2\sigma$, some points still remain outside the shadowed areas. The years corresponding to these outliers are 2009 and 2003. Therefore, we double checked the bi-Gaussian fittings for these years.

Figure 5 shows the bi-Gaussian fitting for solar wind speed for the year 2009. Contrary to expectations, the height of the

Table 5. Typical values for the main parameters of the slow and fast component of the solar wind according to the results from this study.

	V_p (km s^{-1})	B (nT)	n_p (cm^{-3})	T_p ($\times 10^5$ K)
Slow wind	380 ± 40	4.8 ± 0.7 $^{(M)}$ 3.3 ± 0.3 $^{(m)}$	7 ± 1 $^{(M)}$ 4.8 ± 0.5 $^{(m)}$	0.5 ± 0.6
Fast wind	500 ± 100	7 ± 1 $^{(M)}$ 5.6 ± 0.6 $^{(m)}$	3.5 ± 0.8 $^{(M)}$ 2.4 ± 0.2 $^{(m)}$	1.0 ± 0.8

Notes. The years included as the solar maximum (minimum) period are from 1998 to 2003 and from 2011 to 2016 (from 2006 to 2010). $^{(M)}$Maximum solar cycle. $^{(m)}$Minimum solar cycle.

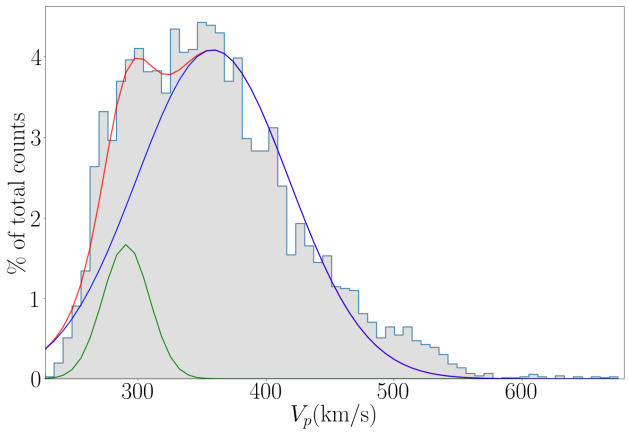

Fig. 5. Empirical distribution functions of the solar wind speed, V_p, recorded by ACE during year 2009 and the fitting to a bi-Gaussian (red). Green and blue lines correspond to the single Gaussian curves.

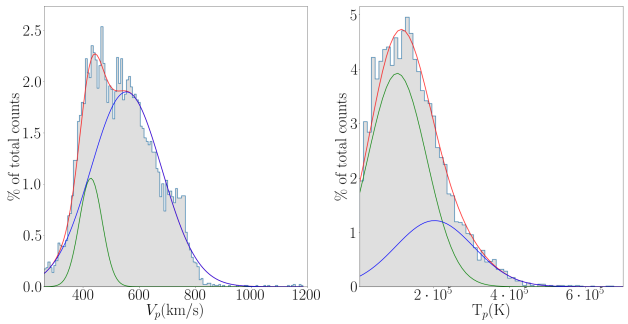

Fig. 6. Empirical distribution functions of the solar wind speed, V_p, (*left*) and proton temperature T_p (*right*) recorded by ACE during year 2003 and the fitting to a bi-Gaussian (red). Green and blue lines correspond to the single Gaussian curves.

peak of the first Gaussian curve is very small when compared to that of the second one. During this year, the Sun was extremely quiet and the amount of flux from coronal holes was negligible. Therefore, the Gaussian with the greatest height, namely the second one, is the one corresponding to the slow solar wind for 2009. Moreover, the first Gaussian can be considered in this case as a mathematical artifact. Indeed, the fitting to a bi-Gaussian of the PDF for the speed in 2009 does not significantly improve the fit to a unique Gaussian.

A different example is that of the year 2003. During that year the Sun was extremely active with a major contribution from fast streams and from solar ejections. Moreover, interaction between different transients happened very often during this year. As a result, other types of wind different from the slow and the fast one contribute significantly to the PDF. The effect of this new population results in an increase of the value of the centre of the peak of both Gaussian curves for proton temperature and solar wind speed (Fig. 6). Thus, this increase in p_1 and p_2 should not be associated to a different value for the typical V_p or T_p due to the slow and fast wind but to a spurious contribution.

After the deep analysis of the bi-Gaussian curves obtained for the years 2003 and 2009 for V_p and T_p, we conclude that an uncertainty of $\pm 2\sigma$ for the weighted average of p_1 and p_2 will be appropriate to describe typical values for these solar wind parameters. Therefore, we recap the typical values for solar wind in Table 5.

5. Conclusions

Here we show that the bi-Gaussian function reproduces the bulk solar wind at 1 AU, not only for proton speed, but also for density, temperature and the magnetic field magnitude. This result suggests that the bulk solar wind at 1 AU is bi-modal, with a fast and a slow component. The typical values for the parameters of the two components are summarised in Table 5

A bi-modal solar wind at 1 AU can be explained as emerging from a bi-modal source. This result leads us to the following open question: is there a clear boundary between small coronal holes responsible for slow solar wind and large coronal holes responsible for fast wind?

In the near future, new data from Parker Solar Probe will provide more in-situ observations of the solar wind in the inner heliosphere at different distances of up to 10 solar radii, shortly after the wind leaves the Sun. These new measurements will allow us to analyse the dynamical evolution of the different parameters of the bi-modal solar wind and to answer the above open question.

Acknowledgements. This work was supported by the MINECO project AYA2016-80881-P (including FEDER funds). We thank the ACE SWEPAM and MAG instruments teams and the ACE Science Center for providing the ACE data. We also acknowledge WDC-SILSO, Royal Observatory of Belgium, Brussels for providing the Sunspot Number. C. L. acknowledges to Rahul Sharma for his help with the layout of the figures.

References

Abbo, L., Ofman, L., Antiochos, S., et al. 2016, Space Sci. Rev., 201, 55
Bale, S., Badman, S., Bonnell, J., et al. 2019, Nature, 1
Bothmer, V., & Zhukov, A. 2007, Space Weather-physics and Effects (Springer), 31
Burlaga, L. F. 2001, J. Geophys. Res.: Space Phys., 106, 15917
Burlaga, L., & King, J. 1979, J. Geophys. Res.: Space Phys., 84, 6633
Burlaga, L. F., & Szabo, A. 1999, Space Sci. Rev., 87, 137
Burlaga, L. F., & Viñas, A. F. 2004, J. Geophys. Res.: Space Phys., 109
Consolini, G., Bavassano, B., & De Michelis, P. 2009, Nonlinear Process. Geophys., 16, 265
Feynman, J., & Ruzmaikin, A. 1994, J. Geophys. Res.: Space Phys., 99, 17645
Garton, T. M., Murray, S. A., & Gallagher, P. T. 2018, ApJ, 869, L12
Hansteen, V. 2010, Stellar Winds and Magnetic Fields (Cambridge: Cambridge University Press), 225
Hirshberg, J. 1969, J. Geophys. Res. (1896–1977), 74, 5814
McComas, D., Bame, S., Barker, P., et al. 1998, Space Sci. Rev., 86, 563
Neugebauer, M., & Snyder, C. W. 1966, J. Geophys. Res. (1896–1977), 71, 4469
Smith, C., L'Heureux, J., Ness, N., et al. 1998, Space Sci. Rev., 86, 613
Stansby, D., Horbury, T. S., & Matteini, L. 2018, MNRAS, 482, 1706
Suhov, Y. M., & Kelbert, M. 2014, Probability and Statistics by Example (Cambridge: Cambridge University Press), 1
Venzmer, M. S., & Bothmer, V. 2018, A&A, 611, A36
Veselovsky, I. S., Dmitriev, A. V., & Suvorova, A. V. 2010, Cosm. Res., 48, 113
Vörös, Z., Leitner, M., Narita, Y., et al. 2015, J. Geophys. Res.: Space Phys., 120, 6152
Wimmer-Schweingruber, R., Crooker, N., Balogh, A., et al. 2006, Coronal Mass Ejections (Springer), 177